Electronically Reconfigurable Virtual Joints by Shape Memory Alloy-Induced Buckling of Curved Sheets

Paul Bupe, Jr.[1], Douglas J. Jackson[1], C. K. Harnett[1]

***Abstract*—This paper presents the concept of creating virtual joints in soft robotic structures by modifying the local curvature of non-stretchable thin-walled structures through shape memory alloy (SMA)-based surface actuation. A thin planar flexible material can be stiffened by curving it along one axis, which increases stiffness by increasing the effective thickness. Locally deforming the curved sheet by making a flat region reduces this thickness, creating a defect. The material buckles and bends in a controlled manner at that location under an external force, producing a virtual compliant joint. We use tailored wire placement techniques to embed a continuous SMA wire in a serpentine pattern into denim cloth stiffened by a thin plastic film. When curved, joints can be created in this structure by activating small segments of the SMA wire using Joule heating which induces local curvature, with each of these segments able to exert up to 1.6 N of force. Finally, we present a circuit and algorithm for routing current through any desired SMA wire segment(s). Experimental results show that compliant joints can be created anywhere along the structure, resulting in a reconfigurable system.**

I. INTRODUCTION

In this paper we propose the use of shape-memory alloy (SMA)-based surface actuation to modify the local curvature of curved, thin-walled, inextensible continuum sheets in order to create reconfigurable virtual joints. A thin flat material like paper can be stiffened by uniformly curving it along a single axis into a U-shape, as shown in Fig. 1. This curved shape exhibits anisotropic properties in that it resists bending along the curve due to increased stiffness in the remaining axis. The stiffness of this structure can be altered by creating a small change in shape along the curve such as creating a flat spot which results in buckling, and thus reduced stiffness, under an external force [1].

The use of curvature for stiffness changes has been widely studied in literature [2]–[5] and can also be found in nature such as in fish fins, batoids, and insect wings [6]. A method for creating directional, compliant virtual joints in thin-walled tubes by changing the local surface curvature is proposed by Jiang et al. [2]. Opposing pairs of internal wire tendons are externally actuated to create pinching forces on the surface of the tube, which then alter the local stiffness. This allows for virtual joints to be created in any radial direction with a recovery of the original shape and stiffness upon release. The authors frame this work as a component of a class of soft robots consisting of Soft, Curved, Reconfigurable, Anisotropic

This work is supported by the National Science Foundation [NSF Award #1935324]

[1] Department of Electrical and Computer Engineering, University of Louisville, Louisville, KY, 40292 USA

Corresponding author: C. K. Harnett (e-mail: c0harn01@louisville.edu)

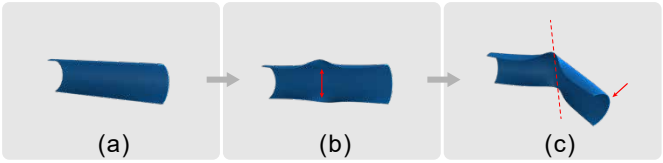

Fig. 1. **Overview and behavior of the Thermally-Actuated SCRAM Limb (TASL).** (a) A thin planar material is curved into a U-shape to create stiffness. (b) Curvature is induced by SMA wire embedded in the surface of the material via tailored wire placement. (c) The structure buckles at the location of the surface curvature under external pressure, creating a joint.

Mechanisms, or SCRAMs. This class of soft robots is able to reconfigure the stiffness of curved surfaces which are then used as virtual joints [2]. Similarly, Jiang et al. [7] are able to create joints in thin-walled tubes along any axis by achieving buckling/pinching through internal negative pressure. They use a movable rigid confining sleeve to control the location and angle of buckling.

Sharifzadeh et al. [6] introduce the concept of using buckling tape springs in order to locomote via flapping fins and wings. They use a compliant, curved beam in between a fin (wing) and an electronic servo. As the servo oscillates, a force is exerted on the end of the beam which causes the curved beam to buckle, effectively creating a joint for half of the flapping cycle that results in large deflections about the buckling point. Drag acts as the restoring force for the compliant, curved beam. The authors are able to tune the buckling behavior of the system by adjusting a number of design parameters including beam length, curvature, and thickness [6].

Our proposed mechanism fits squarely within the SCRAM class of soft robots and expands on the work proposed in [2], [6]. We make use of the aforementioned principles to create a joint anywhere along a continuum curved sheet by creating a surface weakness on the curve using SMA wire and then using an external actuator to force buckling at that location. Our Thermally-Activated SCRAM Limb (TASL) integrates the surface actuators into the material itself in the form of continuous SMA wire in a serpentine pattern, as opposed to using a series of externally actuated wire tendons at a fixed location as in [2]. SCRAMs can be further characterized by the use of planar materials as well as planar fabrication techniques. The addition of using a curved sheet instead of a tube allows for truly planar, and thus simpler, fabrication using well-established tailored wire placement techniques like couching [8]. By placing a continuous wire along the continuum sheet, we are also able to change the location of the joint by actuating

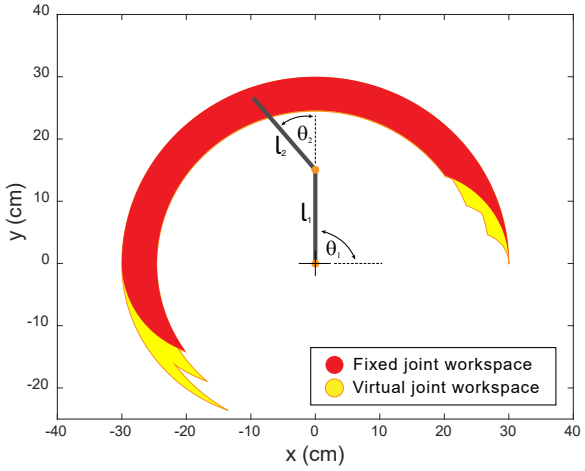

Fig. 2. Workspace comparison between a fixed joint and reconfigurable virtual joint two-link planar arm where $0° < \theta_1 < 180°$ and $0° < \theta_2 < 70°$. The reconfigurable arm given five equally spaced joint locations has a wider reach than the fixed joint arm.

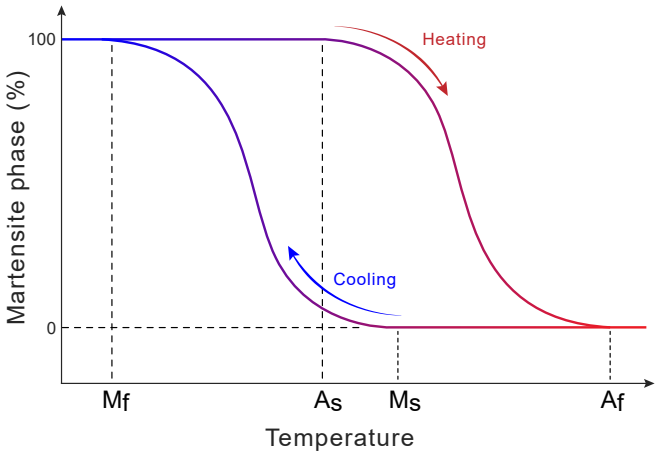

Fig. 3. The heating and cooling cycle of SMAs. As the temperature increases, the atomic lattice structure of SMA wire transitions from the martensite (flexible) state to the austenite (stiff) state. As it cools, it transitions from the austenite state back to the martensite state.

different segments of the continuous SMA wire which results in a reconfigurable system.

A. Reconfiguration

The hysteresis and mechanical nonlinearities of such a reconfigurable system provide many exploitable opportunities, especially in locomotion and manipulation. For example, the TASL with a single virtual joint can be simplified into a 2R planar robotic manipulator with two degrees-of-freedom (DoF), shown in Fig. 2. If the limits on the joint angles of this example manipulator are $0° < \theta_1 < 180°$ and $0° < \theta_2 < 70°$ with the position of the tip given by

$$\begin{bmatrix} x \\ y \end{bmatrix} = \begin{bmatrix} l_1 \cos(\theta_1) + l_2 \cos(\theta_1 + \theta_2) \\ l_1 \sin(\theta_1) + l_2 \sin(\theta_1 + \theta_2) \end{bmatrix} \quad (1)$$

the workspace of this manipulator is contained in the envelope of the plot of the tip positions for all θ_1 and θ_2 angles. Changing the location of the virtual joint changes the value of l_1 and l_2, thus changing the workspace of the manipulator. As shown in Fig. 2, the workspace of the TASL is therefore the union of all the workspaces for each possible virtual joint location. This results in a larger workspace than a similar but fixed-joint manipulator. Looking back to the flapping mechanism proposed by Sharifzadeh et al. [6], being able to control the bending location of the flapping wing would them allow for the option to change the flapping motion of the wing and as a result the overall dynamics of the vehicle, which can be used to optimize for speed or for power efficiency.

B. Shape Memory Alloys

SMAs are useful in soft robotics for their ability to change shape to a known memorized shape when exposed to thermal energy. The training (memorizing) process for SMA wire involves bending it into the desired shape, heating it to a high temperature typically around $400-\ 500\,°\text{C}$, and then letting it cool down. Any subsequent heating near or past its rated activation temperature (which is significantly lower than the training temperature) will cause the SMA wire to attempt to resume its trained shape. This heating can be either external heating or Joule heating by running an electrical current through the wire. There are two general states or phases in which SMAs exist based on their internal crystal lattice structures. In the **cold** martensite phase, the SMA wire is flexible much like a regular solid wire. When heated, the SMA wire's internal structure transitions to the **hot** austenite phase during which the wire stiffens into its trained shape and becomes effectively unbendable, with a spring constant that is 2-3 times higher than in the martensite phase [9]. As illustrated in Fig. 3, heating a SMA causes it to transition from the martensite phase starting at the austenite start temperature (A_s) to the austenite phase ending at the austenite finish temperature (A_f). When cooling, the SMA wire starts transitioning to the martensite phase at the martensite start temperature (M_s) and finishes at the martensite finish temperature (M_f). SMA wire is useful as an actuator because as it heats up and changes its internal structure it contracts $4-8\,\%$, based on the alloy, which can generate significant forces albeit at a short actuation distance. This actuation distance can be increased up to $200-1000\,\%$ by training the wire into a coil spring shape, at the cost of a reduction in force [10]. Nickel-titanium (Nitinol) SMA is the most popular alloy and transitions in the internal crystalline structure under heating changes allow for a $4\,\%$ reduction in length [9].

SMA has been widely used in literature for actuation [10]–[16], hinges for foldable systems [17]–[20], and stiffness tuning layers for soft fluidic actuators [21]. Seok at al. [13] use SMA wire in the design of a soft mobile robotic platform that exhibits peristaltic locomotion – the wire are fabricated into a coil spring actuator whose spring constant is 2-3 times greater in the austenite phase than in the martensite phase. Koh et

al. present a singe-body crawling robot that uses SMA spring actuators to drive two flat four-bar linkages and a folding six-bar linkage [14]. SMA wire is also commonly used to create finger-like actuators that exhibit planar motion. Kim et al. [15] present a finger-like actuator with SMA wire tendons embedded in PDMS that uses soft hinges to increase the bending deformation while Jin et el. [16] also use multiple SMA wires embedded in a rectangular PDMS structure that exhibits bidirectional planar motion. SMAs see wide use in textiles and are one of the most mature fields in active textiles [9], [22]–[24]. Buckner et al. [8] use SMA wire as an actuating fiber trained to create in-plane bending motion in a fabric substrate that is able to present antagonistic motion if paired with a similar actuator on the other side of the fabric. The authors note a major challenge with integrating wire bending actuators into flexible fabric is the tendency for the wire to twist the fabric instead of bending in-plane, caused by any off-center forces, which they alleviate by flattening the round SMA wire into a rectangular profile via annealing and rolling.

There are a number of drawbacks to using SMA wire that need to be overcome in order for it to be a feasible option including the relatively low usable strain, controllability, accuracy, actuation frequency, and energy efficiency [11]. Similar to [8], the SMA wire in the TASL is used to create in-plane bending motion for surface actuation but without the need for rolling the SMA wire to flatten it and with no additional training needed other than the default factory straight training the wire receives during the manufacturing process. Using it in this way allows for large deflections even without training as a spring. Unlike most SMA actuator application, the TASL uses SMA wire not as the primary actuator but only momentarily for the purpose of altering surface curvature so there is no need for great accuracy; this also results in greatly diminished power requirements. Finally, the use case of SMA wire in the TASL does not require precise closed-loop temperature control or fast actuation cycles so those two considerations are not of great import.

C. Primary Contributions

The primary contributions of this paper are as follows:

1) We show that untrained SMA wire can be used as a surface actuator to induce buckling in curved thin-walled structures in order to create a compliant joint. This joint can be created anywhere along the continuum structure by actuating different segments of a continuous SMA wire.
2) We present a layout pattern for untrained SMA wire to be used as a surface actuator and characterize the behavior of this layout.
3) We design a circuit and develop an associated control algorithm for selecting an arbitrary number of segments to activate and demonstrate through an experiment that our proposed mechanism can create virtual joints in different locations.

For the reminder of this paper we first cover the design and fabrication of the TASL in Section II, with special consideration to the material selection. We then characterize, in Section II-B, the surface actuation behavior of the SMA wire and the forces generated by a segment. Next in Section III, we design a multi-channel SMA wire driver circuit and propose an algorithm for activating any segment or combination of segments using our circuit. Finally, we design an experiment to validate the proposed virtual joint and reconfiguration properties of the TASL in Section IV and conclude the paper in Section V.

II. Design and Characterization

In this section we explore the physical specifications, material selection, and fabrication of the TASL. As earlier mentioned, one of the advantages of the TASL is that it uses planar fabrication techniques so fabrication is fairly simple, fast, and accessible. The TASL consists of a layer of fabric, a layer of thin plastic acting as a stiffener and finally SMA wire in a serpentine pattern (Fig. 4), with planar dimensions of $250\,\mathrm{mm}$ x $100\,\mathrm{mm}$. The SMA wire was laid out in a serpentine pattern with each segment $80\,\mathrm{mm}$ long, $8\,\mathrm{mm}$ apart, and with $4\,\mathrm{mm}$ radius corners. The core of the design relies on the use of SMA wire as a surface actuator so the selection and layout of the SMA wire was an important design parameter.

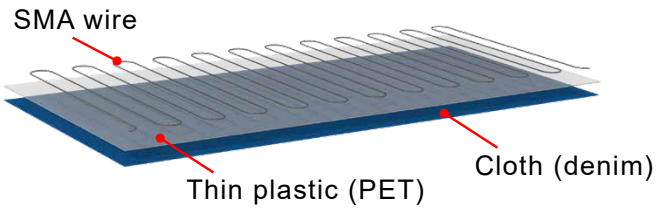

Fig. 4. The TASL is constructed from two material layers, denim cloth and a stiffening PET plastic with SMA wire embedded into the materials using tailored wire placement.

A. Material Selection

1) SMA Wire: There are a number of important parameters to consider when selecting SMA wire such as the alloy, activation temperature, and wire diameter. Nitinol is the best choice of SMA alloy for most applications due to its great stability and thermomechanical properties as opposed to copper and iron-based alloys [11]. The selection of activation temperature depends on the environment and power requirements of the application. For instance, SMA wire that comes in contact with human skin needs to have an activation temperature low enough to not cause burns but high enough that body heat will not activate it. Another important consideration is hysteresis, which is the difference between the heating and cooling transition temperatures given by $\Delta T = A_f - M_s$. We selected SMA wire with an activation temperature of $40\,^{\circ}\mathrm{C}$ and a nominal $0.50\,\mathrm{mm}$ diameter. The selected activation temperature allowed for fast heating with an electrical current while the small diameter enabled for faster cooling.

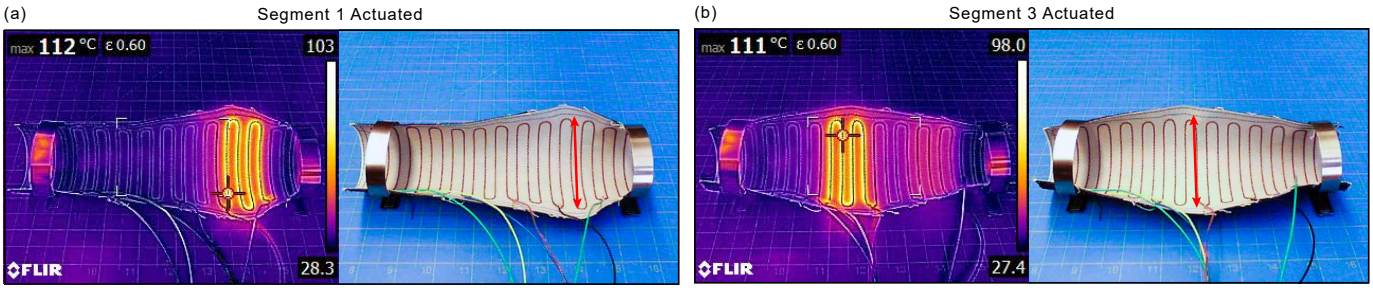

Fig. 5. **Fundamental behavior of the TASL.** When an SMA wire segment is actuated, it stretches and creates a flat spot in the curved surface which allows for controlled buckling to create joints.

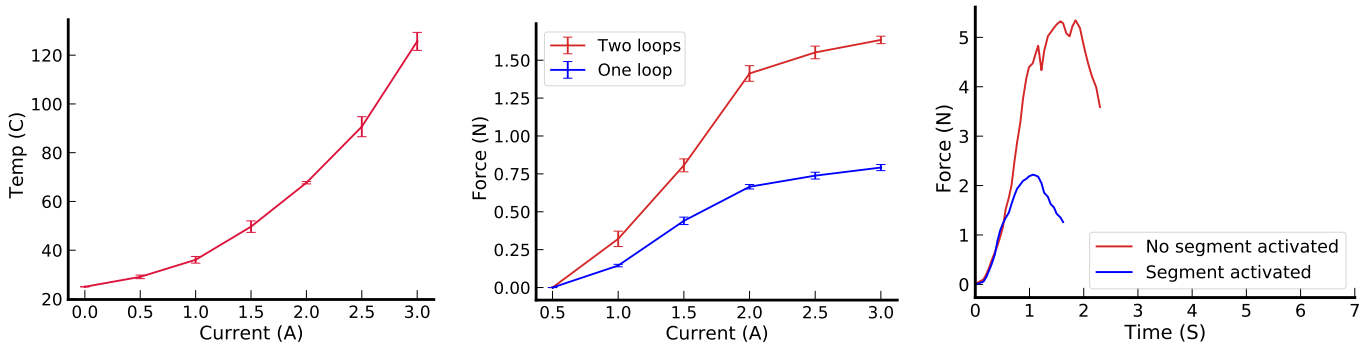

(a) SMA wire temperature vs current.

(b) Patch tip blocking force vs current.

(c) Buckling force.

Fig. 6. **Characterization and testing results of the TASL** (a) This plot correlates current to temperature since SMA is activated by heat but the TASL runs current through the wire to create heat. (b) The maximum tip blocking force scales linearly with the number of loops. (c) The force (normal to the tip) at which the TASL buckles is reduced from $5.35\,\mathrm{N}$ to $2.22\,\mathrm{N}$ after surface actuation. All tests were performed at $22.8\,^{\circ}\mathrm{C}$ and standard environmental condition (static air, atmospheric pressure).

2) Planar Material: In our material selection we sought to find a thin, inextensible, planar material that had the ability to bend without creasing while also providing enough rigidity to maintain a curved shape. This material also needed to be compliant enough to be actuated by the SMA wire. Initially, we embroidered the SMA wire directly onto the denim fabric which yielded poor results when attempting to configure it into a curved shape. The SMA-embedded denim would simply fold over itself and wrinkle up without maintaining shape which meant that a stiffening layer was needed. We then evaluated TPU with a nominal thickness of $0.67\,\mathrm{mm}$. Upon placing the SMA wire and attempting to curve the material we found that even with the added structural rigidity of the serpentine SMA wire pattern the TPU was too soft and the curved U-shape did not propagate along the structure. Attempting to bend it resulted in the structure crumpling in random locations. Next we tried a more rigid frosted Mylar (PET) film with a nominal $0.52\,\mathrm{mm}$ thickness. With the SMA wire in place, this material was found to have the necessary rigidity to form a curved structure and also fold without crumpling. The PET film had a tendency to sometimes create sharp creases so we first stretched a layer of denim under the PET before placing the wire. This layer of denim stretched under the PET had the effect of keeping the bends smooth and constraining the crease to a small radius instead of a sharp end.

B. Characterization

1) SMA Wire Current vs. Temperature: Since we utilized Joule heating to activate the SMA wire, we first characterized the effect of current on the temperature of the wire. Under test was an $8\,\mathrm{cm}$ piece of SMA wire with a cross-sectional diameter of $0.5\,\mathrm{mm}$ and resistance of $300\,\mathrm{m\Omega}$. Current was fed into the SMA wire in increasing increments and the steady-state temperature measured using a FLIR E6 thermal camera with emissivity $\epsilon = 0.60$. The results are plotted in Fig. 6a with $n = 3$. Our SMA wire takes approximately $1\,\mathrm{A}$ to reach the rated $40\,^{\circ}\mathrm{C}$ activation temperature even though the A_s temperature is less than $40\,^{\circ}\mathrm{C}$. On average it took less than 3 seconds to reach temperature.

2) Blocked Bending Force: In order to better characterize the forces generated by each segment of the TASL, we fabricated two patches that contained one and two loops, respectively, of the serpentine pattern with the two-loop patch shown in Fig. 7a. The behavior of the patches is such that when the SMA wire is not activated, the patch can be moved freely and bent or curved into any position as shown in Fig. 7b. When current is applied, the patch straightens out into a flat sheet whose stiffness depends on the rigidity of the SMA wires (EI) [8]. The speed at which the patch straightens out positively correlates with the applied current, which allows for the actuation force of the patch to measured. This force

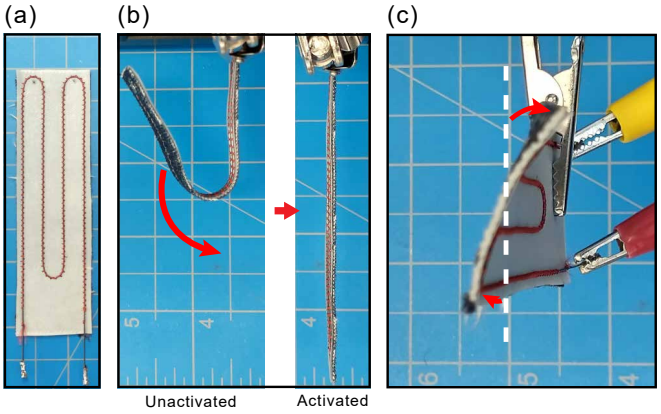

Fig. 7. **Characterization of the SMA wire patch which represents a single segment out of the continuous SMA wire serpentine pattern utilized in the TASL.** (a) Example of the SMA wire patch with two loops. (b) The behavior of the SMA wire patch before and after activation. (c) The twisting behavior of the patch when fully activated.

was measured using the blocked bending tip force test. Each patch was firmly affixed on one end, leaving $10\,\mathrm{cm}$ of the patch for actuation. The free end was bent until the patch was curved into a U-shape with a $2.4\,\mathrm{cm}$ opening (diameter). An end cap that spanned the width of the patch was 3D-printed and attached to the tip of the patch (making contact with the SMA) and a piece of rigid wire was attached to the end cap, passed through an opening in the fixed end of the patch, and connected to a Nextech DFS20 force gauge. The steady-state force was recorded for increasing levels of current, shown in Fig. 6b. The single-loop patch converged to a maximum steady-state $0.8\,\mathrm{N}$ of force while the double-loop reached a steady-state $1.6\,\mathrm{N}$ by $3\,\mathrm{A}$. These results indicate that the max force increasing linearly with the loop count.

3) Surface Actuation: As the forces increased, the patch would exhibit twisting at the free end as shown in Fig. 7c. This behavior can be caused by any off-center forces causing the wire to twist rather than bend and is typically undesired behavior. In fact, Buckner et al. [8] went to significant effort to prevent twisting by physically flattening the SMA wire and training it to bend in-plane. For our application this bending is highly desired because it forces the material to temporarily crease which encourages buckling and thus the formation of a joint. To test the behavior of the patch as a segment within the full continuum structure we attached six evenly-spaced wires to the SMA wire such that there were two loops between pairs of wires, much like the patch. As shown in Fig. 5, we also fit circular clamps at each end to induce camber and thus curving in the TASL. In order to better see the thermal behavior when activated, we captured images using a thermal camera as well as a regular camera. Figs. 5a and 5b show that the SMA is able to significantly actuate the material in different areas based on which segment is active. There is also very little heating of the adjacent areas, below the activation temperature. This test was able to validate the behavior of the patch in its tendency to want to flatten when activated.

III. Control

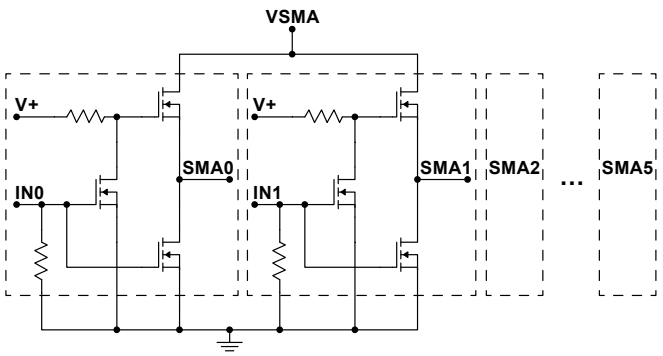

Fig. 8. Simplified SMA wire segment driver circuit showing two of the six channels. For each channel, two MOSFETs are used to reference the channel to either ground or the positive VSMA.

A. Hardware Control

The SMA wire segments are energized by the controlled routing of current through a segment using a MOSFET switch circuit. The fundamental operation of this circuit is to be able to switch a node (an SMA wire in this case) from ground potential to positive and vice versa, effectively creating a SPDT switch. As shown in Fig. 8, this is achieved by using two matched MOSFETs in series, with the controllable node taken in between the MOSFETs. The gates of the two MOSFETs are wired to follow the exclusive-OR behavior such that the only two valid states are when one and only one of the two MOSFETs is on. When the top MOSFET is on and the bottom is off, the controllable node is at positive potential and inversely when the top MOSFET is off and the bottom is on, the controllable node is at ground potential. In this way the controllable node can act as a current source or sink for the SMA wire segment. This base switch circuit is repeated six times in order to control the five SMA segments since n segments require $n+1$ switch circuits. The full circuit was made into a PCB which was designed to be mounted to and controlled by an Arduino Mega microcontroller.

B. Control Algorithm

Since TASL is a continuum mechanism capable of having an arbitrary number of segments, we developed an algorithm for determining which mode (source or sink) to set each node to in order to activate any desired segment(s). Each of the six nodes in the circuit can be represented as a single bit in a 6-bit binary number, with the rightmost node representing *bit* 0. A segment is therefore represented as a pair of adjacent bits, with *Segment 1* corresponding to bits 0 and 1. This definition also means a TASL with n nodes will have $n-1$ controllable segments, as earlier mentioned. Using this scheme, a segment is energized when there is a transition from 0 to 1 or 1 to 0 between adjacent bits. Electrically, this represents a difference in electrical potential and thus a flow of current through that segment, which is visualized in Fig. 10.

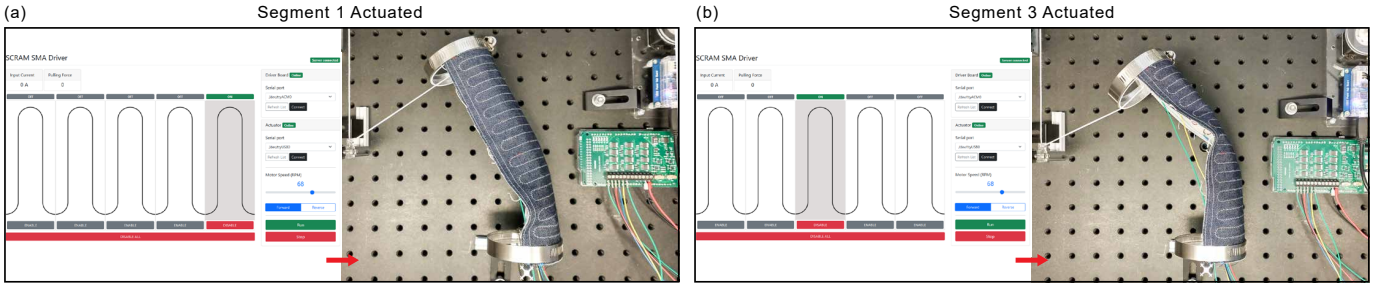

Fig. 9. **A demonstration of the TASL with different joint locations.** (a) A joint formed with *Segment 1* activated. (b) A joint formed with *Segment 1* activated.

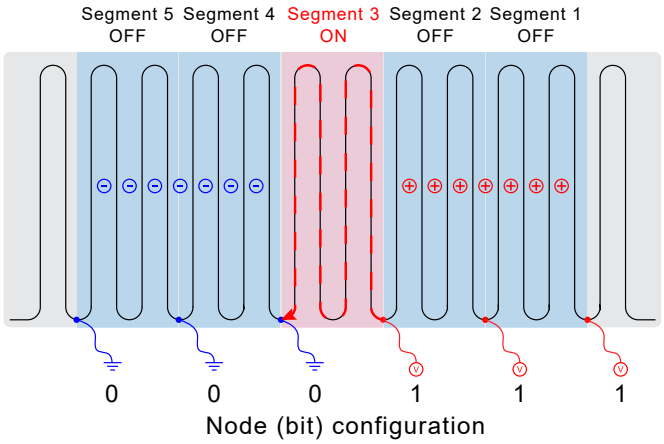

Fig. 10. Visualization of the technique used by the control algorithm to activate a segment of SMA wire along the continuum by creating a potential difference between adjacent nodes.

The binary number $\mathcal{K}$ that represents the bit configuration needed to energize segment m is defined as

$$\mathcal{K} = 2^m - 1 \qquad m \geq 1 \tag{2}$$

As an example using this definition, $\mathcal{K}$ for energizing *Segment 3* is found to be

$$\mathcal{K}_3 = 2^3 - 1 = 7 = b000111 \tag{3}$$

The only transition between a 0 and 1 in this binary number occurs on the two bits representing segment 3, thus segment 3 is energized as visualized in Fig. 10. Energizing multiple segments is then achieved by taking the Exclusive-OR of the $\mathcal{K}$-values of all the segments that need to be energized, given by

$$\mathcal{K}_1 \oplus \mathcal{K}_2 \oplus \cdots \mathcal{K}_n \qquad n \in S \tag{4}$$

where S contains the segment numbers that need to be energized.

IV. Experimental Evaluation

In this section we evaluate the TASL for its ability to create reconfigurable virtual joints. The goal of the prototype was to demonstrate the successful creation of a virtual joint whose position could be reconfigured. Two $5\,\mathrm{cm}$ diameter end caps were laser cut out of $0.635\,\mathrm{cm}$ acrylic which where then used as end caps for the limb, fastened together using a stainless steel hose clamp. The assembled TASL was mounted horizontally on one end with a string attached to the opposite end to be used for external actuation of the limb. Control of the arm was achieved using the aforementioned hardware and a custom software solution. The SMA driver PCB communicated via USB serial to a local Linux control server. This control server also hosted the HTML-based graphical user interface (GUI) used to control the hardware and facilitated duplex communication between the UI and the hardware. Finally, a Dynamixel MX-28 actuator was used as the external actuating force, using a string and pulley system to force buckling in the TASL and create joints.

Results show that the TASL was able to achieve the stated goal of creating virtual joints at different locations. First to validate the reduction in stiffness after surface actuation, we applied a constant pulling force normal to the top plane of the TASL until it buckled. This was the equivalent of putting a weight on top of a half-cylinder. We performed this experiment first without any segments actuated and then with *Segment 3* actuated. Results in Fig. 6c show that SMA surface actuation resulted in a $3.1\,\mathrm{N}$ reduction in the force required to cause buckling. The buckling for the actuated test was also much more smooth and controlled as opposed to the unactuated test.

Next, we reconfigured the test setup such that the initial pulling force was at an approximately $45°$ angle as shown in Fig. 9. When we activated *Segment 1* (Fig. 9a) as hypothesized the TASL buckled at that point which allowed for a joint to form. Upon releasing the pulling force, the TASL reverted to it's flat position under its own power due to the elasticity of the combined materials creating a natural restoring force. Next, we activated *Segment 3* and repeated the same procedure. Once again the TASL buckled at the location of the activated segment and created a joint under an external force (Fig. 9b).

V. Conclusions and Future Work

This paper introduced and validated the use of SMA wire to modify the local surface curvature of curved, thin-walled sheets in order to create reconfigurable virtual joints. Our mechanism belongs to a class of soft robots that are Soft, Curved, Reconfigurable, Anisotropic Mechanisms, or

SCRAMs. In developing the Thermally-Activated SCRAM Limb (TASL), we first showed how untrained SMA wire can be used effectively as a surface actuator despite its known drawbacks and limitations. We then characterized the behavior of SMA wire when tailored into a U-shaped patch, which was a tendency to flatten out regardless of the initial shape. This U-shape was extended into a continuous serpentine pattern that spanned the length of the material. Our testing showed that two loops of this serpentine pattern were able to exert up to $1.6\,\mathrm{N}$ of force, which is enough to bend most planar compliant materials. Finally, we validated the concept with a reconfiguration demonstration successfully showing the creation of joints at different locations. The TASL shows great promise in its simplicity in both concept and fabrication. The nonlinearities and reconfiguration capabilities of such a system allow for the creation of simple yet advanced variable DoF robots. Finally, the use of planar material and fabrication techniques are a new direction in soft robotics and provides many opportunities for advancement in both mechanisms and sensor technologies.

Our future work will focus primarily on the characterization of the surface deformations created by the SMA wire, integrating soft sensors, and evaluating more planar materials. Having a better understanding of how the local curvature modification induces buckling will allow us to better optimize the SMA wire layout which will in turn reduce energy requirements. Since the shapes created on the material at the point of buckling are complex, we plan on using photogrammetry techniques to capture highly detailed 3D surface scans when can then be used to perform analysis and for simulation. Secondly, a sensor will be needed to provide information on the location as well as angle of the bending. This sensor data will be critical in verifying the behavior of the TASL since as a continuum robot it does not have the typical constraints of a rigid-body robot. Finally, we plan on evaluating more materials to find the materials that provide the right balance between compliance and rigidity when curved. Another key obstacle we have to overcome in material selection is that of durability from constant bending. To that end, we seek compliant materials and composites that strongly resist creasing while simultaneously being stiff enough to maintain curvature under operating loads.

REFERENCES

[1] S. Timoshenko and J. Gere, *Theory of Elastic Stability*. Dover Publications, Inc, 2009.

[2] Y. Jiang, M. Sharifzadeh, and D. M. Aukes, "Reconfigurable soft flexure hinges via pinched tubes," in *2020 IEEE/RSJ International Conference on Intelligent Robots and Systems (IROS)*, pp. 8843–8850, ieeexplore.ieee.org, Oct. 2020.

[3] K. Nguyen, N. Yu, M. M. Bandi, M. Venkadesan, and S. Mandre, "Curvature-induced stiffening of a fish fin," *Journal of the Royal Society, Interface / the Royal Society*, vol. 14, May 2017.

[4] V. Pini, J. J. Ruz, P. M. Kosaka, O. Malvar, M. Calleja, and J. Tamayo, "How two-dimensional bending can extraordinarily stiffen thin sheets," *Scientific reports*, vol. 6, p. 29627, July 2016.

[5] N. P. Bende, A. A. Evans, S. Innes-Gold, L. A. Marin, I. Cohen, R. C. Hayward, and C. D. Santangelo, "Geometrically controlled snapping transitions in shells with curved creases," *Proceedings of the National Academy of Sciences of the United States of America*, vol. 112, pp. 11175–11180, Sept. 2015.

[6] M. Sharifzadeh and D. M. Aukes, "Curvature-Induced buckling for Flapping-Wing vehicles," *IEEE/ASME Transactions on Mechatronics*, vol. 26, pp. 503–514, Feb. 2021.

[7] M. Jiang, Q. Yu, and N. Gravish, "Vacuum induced tube pinching enables reconfigurable flexure joints with controllable bend axis and stiffness," in *2021 IEEE 4th International Conference on Soft Robotics (RoboSoft)*, pp. 315–320, Apr. 2021.

[8] T. L. Buckner, R. A. Bilodeau, S. Y. Kim, and R. Kramer-Bottiglio, "Roboticizing fabric by integrating functional fibers," *Proceedings of the National Academy of Sciences*, vol. 117, pp. 25360–25369, Oct. 2020.

[9] T. L. Buckner and R. Kramer-Bottiglio, "Functional fibers for robotic fabrics," *Multifunctional Materials*, vol. 1, p. 012001, Aug. 2018.

[10] RodrigueHugo, WangWei, HanMin-Woo, K. J. Y, and AhnSung-Hoon, "An overview of shape memory Alloy-Coupled actuators and robots," *Soft Robotics*, Mar. 2017.

[11] J. Mohd Jani, M. Leary, A. Subic, and M. A. Gibson, "A review of shape memory alloy research, applications and opportunities," *Materials & design*, vol. 56, pp. 1078–1113, Apr. 2014.

[12] M. Sreekumar, T. Nagarajan, M. Singaperumal, M. Zoppi, and R. Molfino, "Critical review of current trends in shape memory alloy actuators for intelligent robots," *Industrial Robot: An International Journal*, vol. 34, pp. 285–294, Jan. 2007.

[13] S. Seok, C. D. Onal, K. Cho, R. J. Wood, D. Rus, and S. Kim, "Meshworm: A peristaltic soft robot with antagonistic nickel titanium coil actuators," *IEEE/ASME Transactions on Mechatronics*, vol. 18, pp. 1485–1497, Oct. 2013.

[14] J.-S. Koh and K.-J. Cho, "Omega-Shaped Inchworm-Inspired crawling robot with Large-Index-and-Pitch (LIP) SMA spring actuators," *IEEE/ASME Transactions on Mechatronics*, vol. 18, pp. 419–429, Apr. 2013.

[15] H.-I. Kim, M.-W. Han, S.-H. Song, and S.-H. Ahn, "Soft morphing hand driven by SMA tendon wire," *Composites Part B Engineering*, vol. 105, pp. 138–148, Nov. 2016.

[16] H. Jin, E. Dong, M. Xu, C. Liu, G. Alici, and Y. Jie, "Soft and smart modular structures actuated by shape memory alloy (SMA) wires as tentacles of soft robots," *Smart Materials and Structures*, vol. 25, p. 085026, July 2016.

[17] A. Firouzeh, Y. Sun, H. Lee, and J. Paik, "Sensor and actuator integrated low-profile robotic origami," in *2013 IEEE/RSJ International Conference on Intelligent Robots and Systems*, pp. 4937–4944, Nov. 2013.

[18] E. A. Peraza-Hernandez, D. J. Hartl, and R. J. M. Jr, "Design and numerical analysis of an SMA mesh-based self-folding sheet," *Smart Materials and Structures*, vol. 22, p. 094008, Aug. 2013.

[19] J. K. Paik, E. Hawkes, and R. J. Wood, "A novel low-profile shape memory alloy torsional actuator," *Smart Materials and Structures*, vol. 19, no. 12, p. 125014, 2010.

[20] J. K. Paik and R. J. Wood, "A bidirectional shape memory alloy folding actuator," *Smart materials & structures*, vol. 21, p. 065013, May 2012.

[21] F. Schmitt, O. Piccin, L. Barbé, and B. Bayle, "Soft robots manufacturing: A review," *Frontiers in robotics and AI*, vol. 5, p. 84, July 2018.

[22] V. Sanchez, C. J. Walsh, and R. J. Wood, "Textile technology for soft robotic and autonomous garments," *Advanced functional materials*, vol. 31, p. 2008278, Feb. 2021.

[23] V. Sanchez, C. J. Walsh, and R. J. Wood, "Soft robotics: Textile technology for soft robotic and autonomous garments (adv. funct. mater. 6/2021)," *Advanced functional materials*, vol. 31, p. 2170041, Feb. 2021.

[24] C. Kim, G. Kim, Y. Lee, G. Lee, S. Han, D. Kang, S. H. Koo, and J.-S. Koh, "Shape memory alloy actuator-embedded smart clothes for ankle assistance," *Smart Materials and Structures*, vol. 29, p. 055003, Mar. 2020.